

## Supramolecular Dual Polypeptides Induced Tubulin Aggregation for Synergistic Cancer Theranostics

Mian Tang,<sup>#</sup> Yao-Hua Liu,<sup>#</sup> Hua Liu, Qiyue Mao, Qilin Yu, Hiroaki Kitagishi, Ying-Ming Zhang,\*  
Lehui Xiao,\* and Yu Liu\*Cite This: *J. Med. Chem.* 2022, 65, 13473–13481

Read Online

ACCESS |



Metrics &amp; More

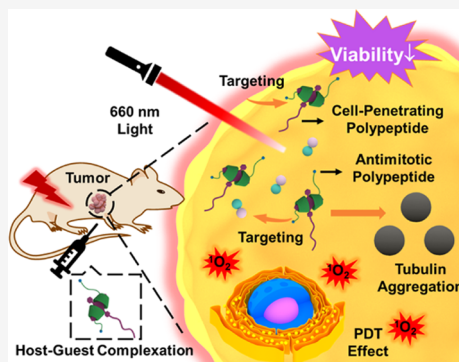


Article Recommendations



Supporting Information

**ABSTRACT:** The advent of macrocycle-based supramolecular chemistry can offer powerful strategies for regulating vital bioactivities in living systems and bring about emerging technology in biomedical science. Herein, we construct a supra-biomacromolecular nanosystem involving microtubules, cell-permeable porphyrins, and antimetabolic peptide-decorated permethyl- $\beta$ -cyclodextrins for promoting cell apoptosis in a cooperative manner. Through specific polypeptide–tubulin recognition, cyclodextrin moieties are capable of anchoring to the tubulin surface and providing abundant hydrophobic microenvironments to accommodate the photosensitive porphyrins. Consequently, spherical tubulin aggregates are formed, and reactive oxygen species can be efficiently generated via the host–guest complexation. The combined usage of complexation-promoted photodynamic efficacy and tubulin aggregation gives more serious cell apoptosis under light irradiation in vitro and in vivo. To be envisioned, this supramolecularly enhanced photodynamic performance together with controlled aggregation of natural biomacromolecules may be developed as an innovative approach to improve the therapeutic potency against many diseases.



## INTRODUCTION

The past few decades have witnessed the substantial development of macrocycle-based supramolecular chemistry from single inclusion complex to multicomponent assembly at different scales and dimensions. No longer content with increasing the water-solubility and biocompatibility of selected substrates, researchers are now vigorously pursuing more reliable methods to regulate the essential living processes by a host–guest interaction. In this context, the combination of macrocycles and biological macromolecules, such as nucleic acids, peptides, and proteins, has been proven as a feasible and powerful means of conferring topologically interesting structures and elaborating functions to a given supramolecular nanosystem.<sup>1–3</sup> On one hand, the embedded macrocycles can make direct noncovalent encapsulation with neighboring subunits of biomacromolecules (e.g., amino acid residues), by which the whole conformation and the concomitant biological consequence can be significantly affected.<sup>4–6</sup> On the other hand, the inherent cavity of macrocycles can offer numerous confined microenvironments as anchoring points in the three-dimensional (3D) structures of biomacromolecules, by which the exogenous substances can be conveniently captured.<sup>7,8</sup> Through leveraging the covalent chemical modification and the noncovalent encapsulation, the coupling of macrocyclic receptors and biomacromolecules has provided bountiful opportunities for fabrication of well-defined topological nanoconstructs.<sup>9–11</sup>

Recently, supramolecular multimodal theranostics by delivering different types of treatments together have been developed as a sturdy tool to overcome the drawbacks associated with single-modality ones.<sup>12,13</sup> By virtue of the noncovalent functionalization approaches, precise diagnosis and personalized therapy can be realized by integrating several building components into a self-assembled entity. Supramolecular nanoformulations arising from multiple intermolecular interactions have shown immense advantages in bioimaging,<sup>14,15</sup> drug delivery,<sup>16,17</sup> and combined therapy,<sup>18,19</sup> which may hold great promise for clinical translation and applications. In particular, the conformational confinement with macrocyclic receptors can dramatically improve the photophysical performance of included chromophores via host–guest complexation. Such host–guest-binding-controlled energy transition pathways are very conducive to the emergence of new light-activated therapeutic methods, which are viewed as typical examples for achieving the synergistic “1 + 1 > 2” effect in the biomedical fields.<sup>20–23</sup>

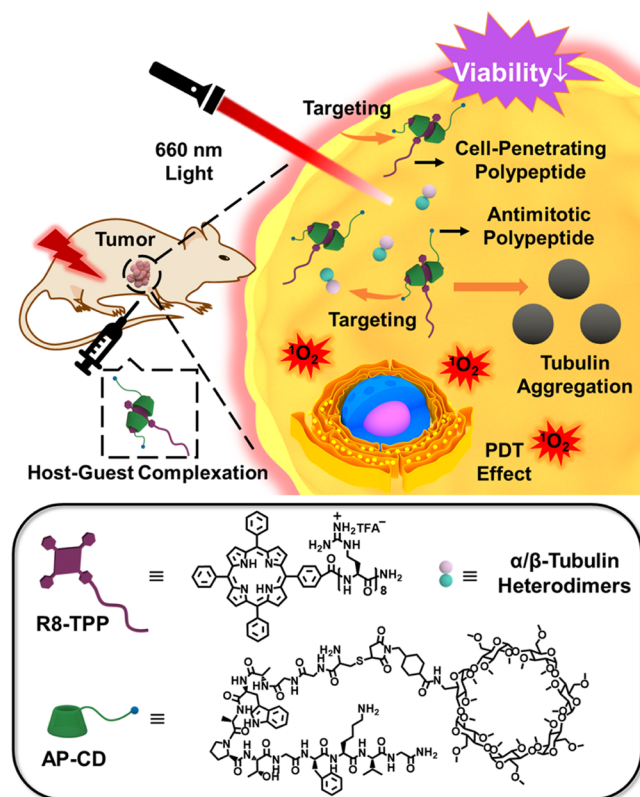
Received: August 24, 2022

Published: September 14, 2022



In this work, we propose a dual polypeptide-involved supramolecular method to specially regulate the cell fate by the cross-linked tubulin aggregation and complexation-enhanced photodynamic efficacy. The globular  $\alpha/\beta$ -tubulin heterodimers are key biomacromolecules in the formation of microtubules, and the assembly behaviors of tubulins are actively involved in many physiological processes.<sup>24,25</sup> The antimetabolic and cell-penetrating polypeptides are covalently attached to the backbones of methylated cyclodextrin (CD) and tetraarylporphyrin, respectively, thus endowing the resultant supramolecular assembly with the desired dual-target ability (Scheme 1). Benefitting from the strong 2:1 host–guest

**Scheme 1. Schematic Illustration of the (R8-TPP@AP-CD)@Tubulin Ternary Supramolecular Assembly for Targeted Tubulin Aggregation and an Enhanced Photodynamic Effect**



complexation, extensive tubulin aggregates are formed, and photosensitized production of singlet oxygen is improved in the cell milieu. As a result, severe cell apoptosis and dramatic cancer ablation have been simultaneously achieved by such a two-step synergistic process. Therefore, it can be envisioned that this work will provide an appealing strategy for establishing effective nanoplatforams for multimodal cancer theranostics at the supra-biomacromolecular level.

## RESULTS AND DISCUSSION

**Synthesis and Host–Guest Complexation Characterization.** The antimetabolic polypeptide-modified permethyl  $\beta$ -cyclodextrin (AP-CD) and the octaarginine-conjugated tetraphenylporphyrin (R8-TPP) were used as host and guest molecules, respectively. The synthetic routes and compound characterization are shown in the Supporting Information (Figures S1–S9). In our case, the tubulin-targeted antimetabolic peptide was chemically modified at its N-terminal via an extra

linkage containing glycine and cysteine residues. These nonbiologically meaningful molecular fragments with a suitable length cannot interfere with the existing peptide–tubulin interaction and host–guest complexation between permethyl  $\beta$ -CD and R8-TPP. Moreover, the conjugation of the  $\beta$ -CD moiety and antimetabolic peptide was achieved using a bifunctional cross-linker, succinimidyl 4-(*N*-maleimidomethyl)cyclohexane-1-carboxylate, via the well-established Michael addition reaction. Compared with other porphyrin derivatives, R8-TPP has excellent membrane penetration ability, good solubility, near-infrared (NIR) fluorescence emission, and efficient ability to generate singlet oxygen as reported by Kitagishi et al.<sup>26</sup> In addition, R8-TPP with a neutral porphyrin core and the condensed positive charges can simultaneously ensure good cell permeability and high inclusion complexation with permethyl  $\beta$ -CD.<sup>27</sup> The construction of the (R8-TPP@AP-CD)@tubulin supramolecular assembly is depicted in Scheme 1.

The host–guest binding behaviors in the inanimate milieu were preliminarily explored by <sup>1</sup>H NMR spectroscopy. As discerned from Figures 1a,b and S10, the proton signals of free R8-TPP underwent significant passivation in the <sup>1</sup>H NMR spectrum, whereas a simple pattern of sharp signals was observed in the presence of PMeCD, suggesting that R8-TPP was dissipated to the monomeric form (or a low aggregated form at most). Meanwhile, there were clear nuclear Overhauser enhancement (NOE) cross-peaks between the aromatic protons of R8-TPP and the  $\beta$ -CD's inner cavity (Figure S11, Supporting Information). Also, by judging from the steady enhancement in UV absorbance and fluorescence emission upon complexation of R8-TPP with PMeCD, we can reasonably infer that the porphyrin core of R8-TPP was exclusively included in the  $\beta$ -CD's cavities (Figures 1c and S12, Supporting Information). Moreover, after validating the 1:2 complexation stoichiometry by the Job plot, the stepwise binding constants ( $K_1$  and  $K_2$ ) could be calculated to be  $1.72 \times 10^4$  and  $1.93 \times 10^5$  M<sup>-1</sup>, respectively, by the nonlinear least-squares curve-fitting method (Figure 1c(inset),1d). Accordingly, the cooperativity factor ( $\alpha$ ) was obtained as 45, indicative of strong positive cooperativity upon host–guest complexation. In addition, <sup>1</sup>H NMR experiments showed that the addition of 10% fetal bovine serum (FBS) had no obvious effect on the binding of PMeCD and R8-TPP (Figure S13, Supporting Information). The complex of R8-TPP@SMCC-CD was stable in phosphate-buffered saline (PBS) solution containing 10% FBS for 5 days (Figure S14, Supporting Information). Apparently, the tight host–guest complexation may facilitate the microtubular aggregation and concomitant photodynamic effect, as described below.

### Efficient Induction of Tubulin Aggregation In Vitro.

Furthermore, the influence of a 2:1 supramolecular cross-linkage between AP-CD and R8-TPP on tubulin aggregation behaviors was intuitively characterized by transmission electron microscopy (TEM). As shown in Figure 2a, the pristine tubulin exhibited uniform nanofibers with a length of several micrometers, corresponding to the spontaneous heterodimerization of  $\alpha/\beta$  tubulins in the general tubulin buffer. Meanwhile, bundles of tubulin nanoribbons were formed upon addition of individual AP-CD and R8-TPP at relatively low concentrations, suggesting that the assembling mode of tubulin is essentially unchanged in these control experiments (Figure 2b,c). The formation of tubulin nanoribbons caused by the addition of AP-CD alone may be due to

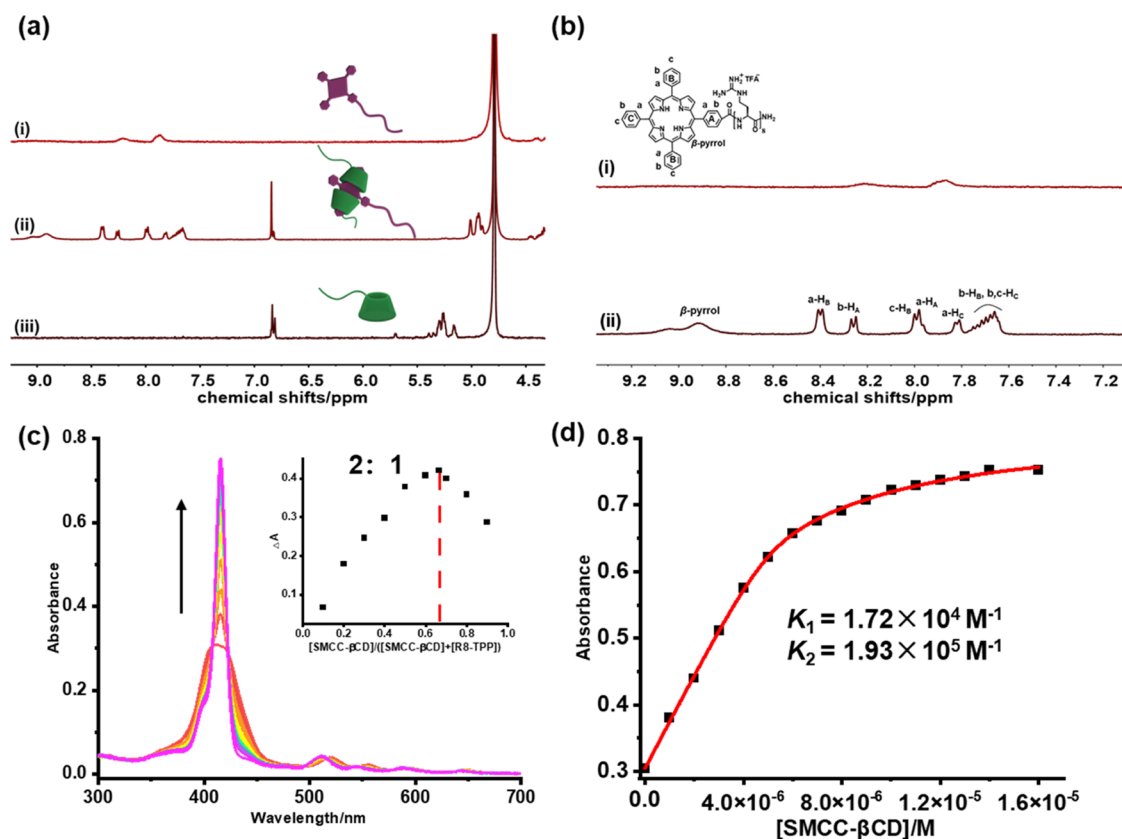


**Figure 1.** (a) Partial  $^1\text{H}$  NMR spectra (400 MHz,  $\text{D}_2\text{O}$ , 25  $^\circ\text{C}$ ) of (i) R8-TPP, (ii) binary complex, and (iii) SMCC- $\beta$ -CD ( $[\text{SMCC-}\beta\text{-CD}] = 2[\text{R8-TPP}] = 2.0 \text{ mM}$ ). (b) Partial  $^1\text{H}$  NMR spectra (400 MHz,  $\text{D}_2\text{O}$ , 25  $^\circ\text{C}$ ) of (i) R8-TPP, (ii) R8-TPP/SMCC- $\beta$ -CD, and (c) SMCC- $\beta$ -CD ( $[\text{SMCC-}\beta\text{-CD}] = 2[\text{R8-TPP}] = 2.0 \text{ mM}$ ). (c) UV-vis spectral changes of R8-TPP upon addition of SMCC- $\beta$ -CD ( $[\text{R8-TPP}] = 5.0 \mu\text{M}$  and  $[\text{SMCC-}\beta\text{-CD}] = 0\text{--}20 \mu\text{M}$ ). (Inset: Job plot of R8-TPP/SMCC- $\beta$ -CD complexation ( $[\text{R8-TPP}] + [\text{SMCC-}\beta\text{-CD}] = 5.0 \mu\text{M}$ )). (d) Nonlinear least-squares analysis of the differential UV-vis absorbances ( $\Delta A$ ) to calculate the  $K_s$  values.

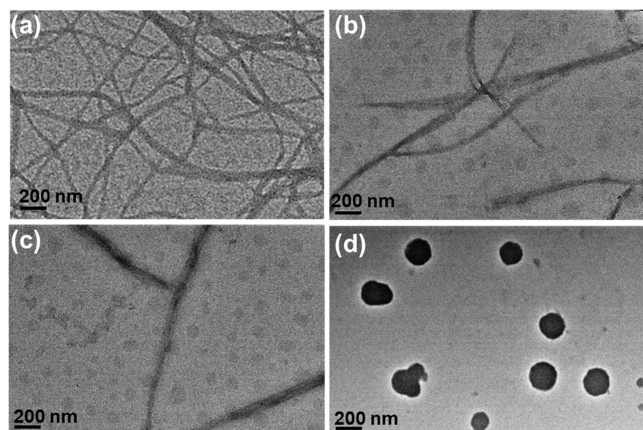


**Figure 2.** TEM images of (a) free tubulin, (b) R8-TPP/tubulin, (c) AP-CD@tubulin, and (d) (R8-TPP/AP-CD)@tubulin ( $[\text{tubulin}] = 1.0 \text{ mg/mL}$ ,  $[\text{R8-TPP}] = 25 \mu\text{M}$ ,  $[\text{AP-CD}] = 50 \mu\text{M}$ ,  $\text{pH} = 6.9$ ). The scale bar in each TEM image is 200 nm.

the peptide-protein interaction between the microtubule-targeted AP and tubulin; while the addition of R8-TPP alone can lead to the formation of tubulin nanobelts, which may be due to the charge interaction between the tubulin and cationic charge-rich cell-penetrating peptide in the molecular structure of R8-TPP. Surprisingly, spherical nanostructures were clearly observed with an average diameter of 220 nm in the case of (R8-TPP/AP-CD)@tubulin, which was attributed to the

microtubular aggregation via multiple host-guest cross-linkages (Figure 2d).

The solid evidence of the host-guest-binding-induced tubulin aggregation came from the high-resolution images obtained by total internal reflection fluorescence microscopy (TIRFM). In this case, given the relatively higher photostability, meso-tetra(4-carboxyphenyl)porphine (TCPP) was chosen as the substitute for R8-TPP. In addition, thioflavin T (ThT), a commonly used fluorescent dye for staining proteins, was employed to light up the tubulin and microtubule in vitro.<sup>28,29</sup> As shown in Figure 3a-c, the addition of TCPP or AP-CD alone could not make any impact on the microtubule morphology, and the filamentlike structures were still maintained. In sharp contrast, when TCPP and AP-CD were added to the buffer solution at the same time, the tubulins were largely clustered (Figure 3d). Meanwhile, the red fluorescence of TCPP and the green fluorescence of ThT were perfectly overlapped with the assistance of tubulin-targeted AP-CD, again corroborating the important role of host-guest complexation in the tubulin aggregation (Figure S15, Supporting Information).

In line with the microscopic observation, there were also significant size changes in the aqueous phase. R8-TPP can make a decrease in the optical transmittance, which should be attributed to the formation of bundles of tubulin nanoribbons shown by TEM experiments. That is, when R8-TPP was added to the solution of CD-pendant tubulins, the optical transmittance dramatically decreased and the hydrodynamic

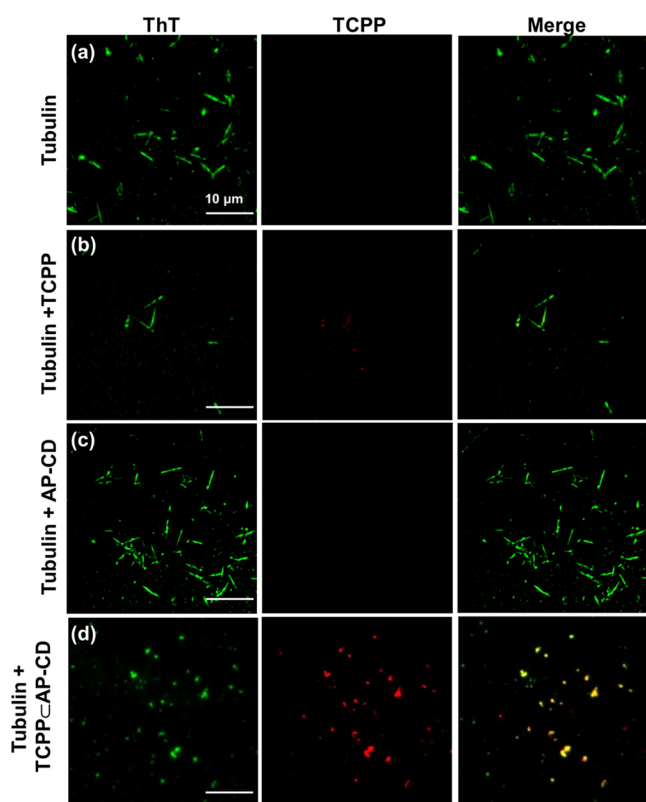


**Figure 3.** TIRFM images of (a) free tubulin, (b) tubulin/TCPP, (c) AP-CD@tubulin, (d) (TCPP@AP-CD)@tubulin assembly stained with ThT. Note that ThT and TCPP were excited at 450 and 532 nm, respectively. ([Tubulin] = 0.01 mg/mL, [TCPP] = 0.5  $\mu$ M, [AP-CD] = 1.0  $\mu$ M, [ThT] = 10 nM, in general tubulin buffer solution, pH = 6.9.) The scale bar in each image is 10  $\mu$ m.

diameter became larger (Figures S16 and S17, Supporting Information), further confirming the formation of large-sized supramolecular aggregates. Taken together, these results unequivocally manifest that a single polypeptide–tubulin interaction is not sufficient enough to alter the tubulin assembling behaviors, and the multiple supramolecular cross-linkage arising from the R8-TPP@AP-CD complexation is considered an indispensable factor for inducing the morphological and size variation in the tubulin aggregation process. Thus, it is expected that the orthogonal peptide–tubulin and host–guest interactions in the (R8-TPP@AP-CD)@tubulin supramolecular system may seriously interfere with the tubulin function at the cellular level.

**Singlet Oxygen Generation.** Subsequently, the singlet oxygen ( $^1\text{O}_2$ ) quantum yields ( $\phi_\Delta$ ) of R8-TPP before and after complexation with AP-CD were measured using 9,10-anthracenediyl-bis(methylene)dimalonic acid (ABDA) as an  $^1\text{O}_2$  indicator and methylene blue (MB) as a reference (Figures S18–S20, Supporting Information). Remarkably, the UV absorbance of ABDA at 380 nm was largely reduced after addition of R8-TPP and the R8-TPP@AP-CD complex under irradiation of 650 nm. Also, as can be seen from Figure S20 (Supporting Information), the rate of singlet oxygen generation from this assembly under light irradiation was improved after the addition of AP-CD, and the  $\phi_\Delta$  value of the R8-TPP@AP-CD complex was 1.3 times higher than that of R8-TPP alone. In addition, the singlet oxygen yield of the R8-TPP@AP-CD complex changed very little in the presence of

tubulin. These results confirmed that the formation of the binary supramolecular assembly could greatly enhance the photodynamic therapy effect of porphyrins.

**Anticancer Activities In Vitro.** Subsequently, confocal laser scanning microscopy was employed to investigate the complexation-induced microtubular aggregation and photodynamic properties in the human lung adenocarcinoma (A549) cells. As shown in Figure 4a(i), the pristine tubulins stained with the tubulin tracker were uniformly distributed around the nucleus. Initially, R8-TPP alone was also widely distributed all over the cytoplasm, indicating that the TPP molecule decorated by the cell-penetrable peptide could be readily internalized but without the targeting ability at the subcellular level (Figure 4a(iii)). Meanwhile, the incubation with AP-CD could not change the cytoskeletal structures (Figure 4a(iv)). In sharp contrast, as discerned from Figure 4a(ii), spherically aggregated tubulins were clearly observed in the selected cell line and the aggregated tubulins stained with green fluorescence perfectly overlapped with the red region of the R8-TPP@AP-CD complex (Figure S21, Supporting Information). As a comparison, A549 cells incubated with R8-TPP, SMCC-CD, and antimetabolic polypeptide (AP) exhibited a normal microtubule morphology, which demonstrated that the synergistic interaction between host–guest and peptide–protein interactions resulted in the abnormal assembly of tubulins (Figure S22, Supporting Information). This abnormal cell morphology induced by extensive supramolecular cross-linkages prompted us to consider its biological effect on cell viability. First, the generation of reactive oxygen species (ROS) was detected in the A549 cells using 6-carboxy-2',7'-dichlorodihydrofluorescein diacetate (DCFH-DA) as an indicator. As can be seen from Figure 4b, bright green fluorescence was observed in the cells, implying that a large amount of ROS could be produced with a high quantum yield by the R8-TPP@AP-CD complex after light irradiation at 650 nm for 10 min. Meanwhile, the R8-TPP@AP-CD complex exhibited remarkable dose-dependent cytotoxicity toward the A549 cells. For example, when the concentration of R8-TPP was fixed at 15  $\mu$ M, the relative cell viability sharply declined to 48.3% in the presence of essentially nontoxic AP-CD, while the cells treated with AP-CD alone were maintained at nearly 100% viability (Figure 4c). Accordingly, the half-maximal inhibitory concentration ( $\text{IC}_{50}$ ) of the R8-TPP@AP-CD complex was calculated as 14.3  $\mu$ M, whereas AP-CD alone showed no significant cytotoxicity in the tested concentration range. In addition, the photocytotoxicity of the R8-TPP@AP-CD complex was also evaluated. Compared with the cells treated in the dark, the ones treated under light irradiation at 650 nm for 5 min gave much lower cell viability (Figure 4d). Under such circumstances, the corresponding  $\text{IC}_{50}$  value could reach as low as 9.2  $\mu$ M. Therefore, owing to the complexation-assisted tubulin aggregation and ROS production, cell apoptosis could be dramatically enhanced at a higher level.

**Inhibition of Tumor Growth by Dual Polypeptide Supramolecular Assembly.** Considering the tubulin disruption and photodynamic properties of the R8-TPP@AP-CD assembly at the cellular level, we were curious to see whether such dual peptide-induced tubulin aggregation and complexation-enhanced photodynamic therapy could be used to achieve efficient cancer theranostics in the animal model. Therefore, Balb/c nude mice bearing an A549 tumor model were established, and peritumoral drug injections and laser irradiation were used to evaluate the treatment outcomes. The

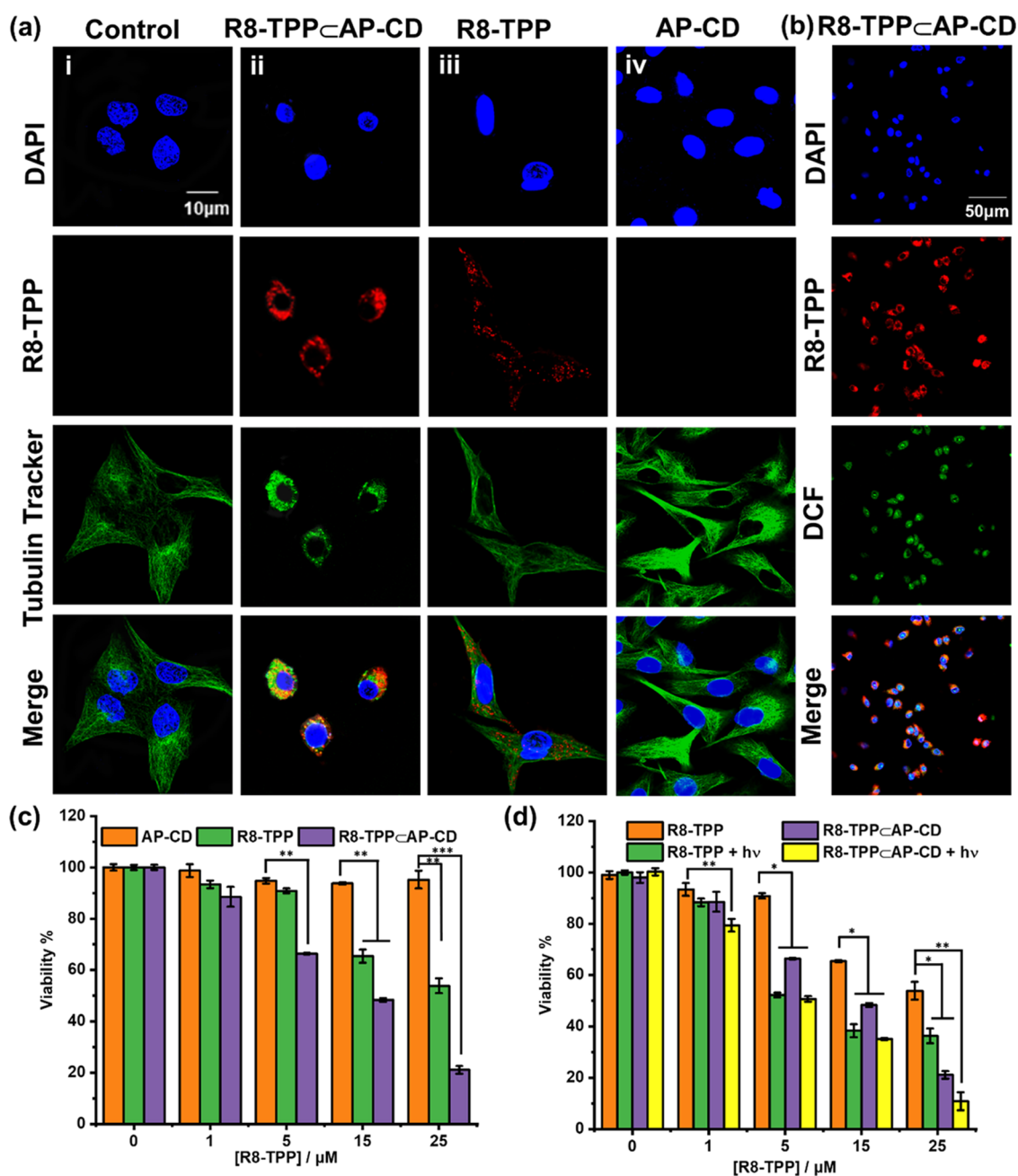


**Figure 4.** (a) Confocal fluorescence images of A549 cells incubated with (i) control, (ii) R8-TPP/AP-CD complex, (iii) R8-TPP, and (iv) AP-CD. The tubulin tracker (green) and 4',6-diamidino-2-phenylindole (DAPI, blue) were used to stain the cytoskeleton and nucleus, respectively. The fluorescence of R8-TPP was red. Note that R8-TPP, tubulin tracker, and DAPI were excited at 633, 488, and 405 nm, respectively. (b) Confocal fluorescence images of A549 cells incubated with. DCFH-DA (green) was used to stain reactive oxygen. The cells were treated with filtered light at 650 nm for 10 min. Note that DCFH was excited at 488 nm. (c) Cell viability inhibition test in the dark by AP-CD and the R8-TPP/AP-CD complex. (d) Photocytotoxicity after incubation with the R8-TPP/AP-CD complex for 12 h followed by the light irradiation at 650 nm for 5 min. Student's *t*-test was used for statistical analysis ( $*p < 0.05$ ,  $**p < 0.01$ ), and all data were expressed as mean  $\pm$  standard error of the mean.

weight of mice in all experimental groups showed a steady increase in body weight, implying that no systemic side effect was found in this supramolecular theranostic system (Figure 5a). Since AP-CD is a biofriendly molecule, the AP-CD treatment group had little therapeutic effect in vivo. In addition, weaker therapeutic effects were shown in the R8-TPP and R8-TPP +  $h\nu$  groups mainly arising from the poor phototoxicity of individual R8-TPP. Also, a certain tumor treatment effect was observed in the R8-TPP/AP-CD complex group, which was attributed to the complexation-induced

tubulin aggregation. Notably, benefiting from the synergistic dual peptide-induced tubulin aggregation and photodynamic therapy, tumor growth was substantially inhibited in the R8-TPP/AP-CD complex +  $h\nu$  treatment group throughout the experimental period (Figure 5b,c). At the same time, due to the strong fluorescence emission of porphyrin, all of the R8-TPP-involved treatment groups could effectively exhibit in vivo fluorescence imaging behaviors (Figure 5d). Finally, the hematoxylin and eosin (H&E) staining of major organs and tumor tissues was performed in mice. No obvious lesion was

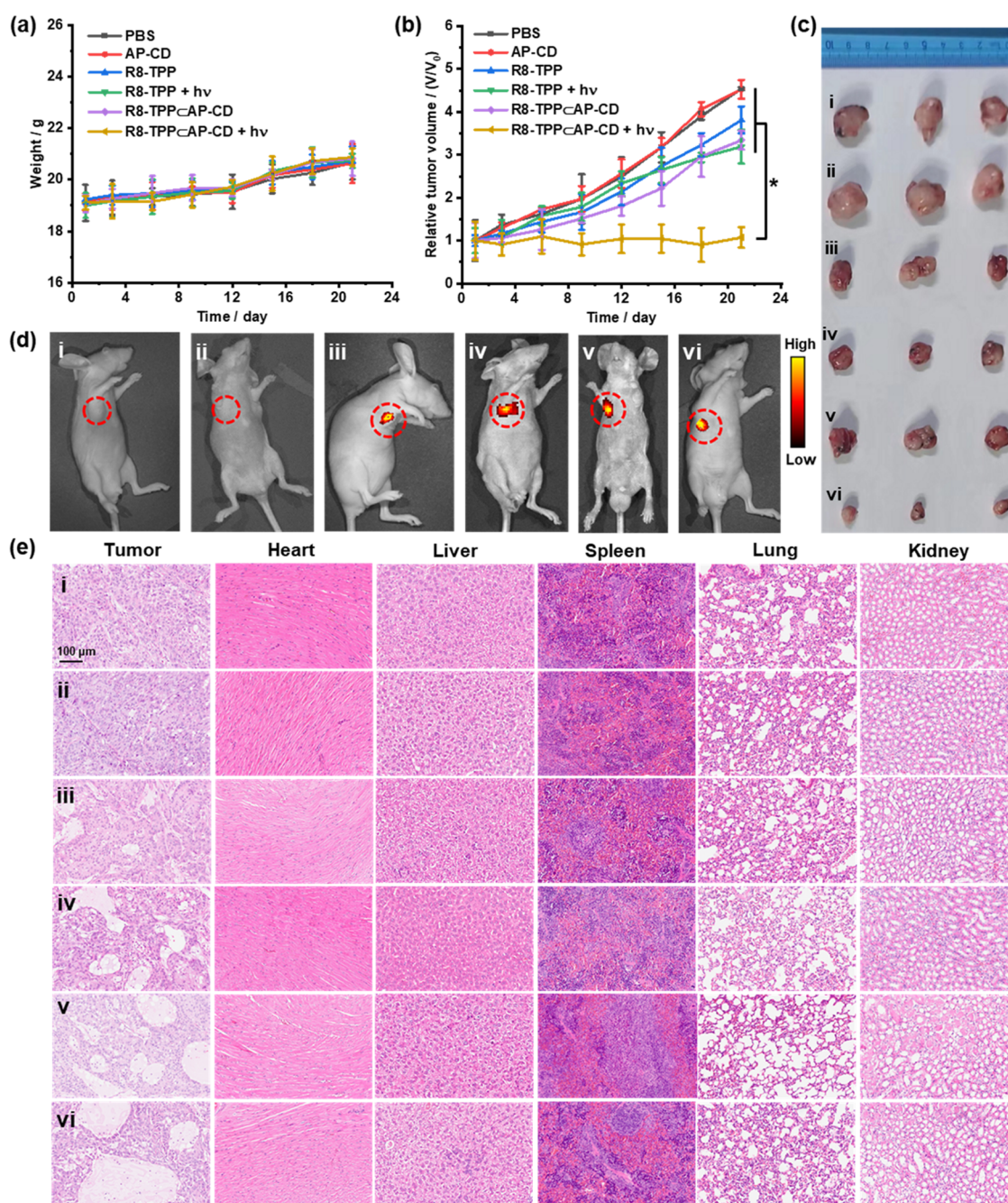


**Figure 5.** (a) Body weights of the mice in different groups after treatment at different time intervals. (b) Time-dependent tumor sizes from different groups of mice with different treatments over a period of 21 days. (c) Representative photographs of tumors at the end of the in vivo anticancer experiments. (d) In vivo fluorescence images of mice with different treatments (i, PBS; ii, AP-CD; iii, R8-TPP; iv, R8-TPP + hv; v, R8-TPP<sub>CD</sub>; and vi, R8-TPP<sub>CD</sub> + hv). Note that R8-TPP was excited at 640 nm. (e) H&E staining of tumor tissues from different samples of euthanized mice. Student's *t*-test was used for statistical analysis ( $*p < 0.05$ ), and all data were expressed as mean  $\pm$  standard error of the mean.

found in the organs of the mice in all treatment groups, which once again confirmed the biocompatibility of the supramolecular treatment strategy. Meanwhile, the R8-TPP<sub>CD</sub> complex + hv treatment group gave the most obvious treatment effect, proving the high efficiency of the supramolecular combinational treatment strategy (Figure 5e). In addition, to increase the targeting of supramolecular assemblies, the supramolecular nanoparticles were constructed using the cancer-cell-specific hyaluronic acid (HA) with the R8-TPP<sub>CD</sub> complex. TEM and dynamic light scattering

(DLS) experiments showed that such ternary supramolecular assemblies formed nanoparticles with a diameter of about 160 nm (Figures S23 and S24, Supporting Information). As expected, the in vivo image of the mouse injected with the supramolecular nanoparticles via the tail vein showed that the NIR fluorescence of the supramolecular assembly can clearly outline the tumor after injecting the assemblies for 8 h (Figure S25, Supporting Information). These experiments can demonstrate that the further assembly of the supramolecular complex of the R8-TPP<sub>CD</sub> complex with HA through

the electrostatic interaction can achieve targeted drug delivery. Overall, these *in vivo* animal experiments jointly demonstrated that the supramolecular dual peptide-induced tubulin aggregation and photodynamic therapy could largely inhibit tumor growth without common systemic adverse effects.

## CONCLUSIONS

In conclusion, the antimetabolic and cell-permeable polypeptides were covalently attached to PMeCD and TPP, respectively, thus endowing the host and guest molecules with the desired dual-targeting ability. The supra-biomacromolecular (R8-TPPCAP-CD)@tubulin assembly could be readily obtained via the orthogonal polypeptide–tubulin recognition and host–guest interaction. In the inanimate milieu, as confirmed by the morphological characterization, nanoparticulate assemblies of tubulins were formed via the stable R8-TPPCAP-CD complexation. In an intracellular environment and an *in vivo* tumor environment, the extensive intermolecular cross-linkage could not only induce tubulin aggregation but also promote the photodynamic effect of included R8-TPP, jointly resulting in more significant cell apoptosis and tumor ablation. The results present in this work demonstrate the innate superiority of the supramolecular strategy involving the dual-targeted polypeptide-induced and host–guest-binding-enhanced tubulin dysfunction and photodynamic outcome, which may be developed as an advanced theranostic method against many degenerative diseases in the future.

## EXPERIMENTAL SECTION

**Materials.** All chemicals were commercially available and used without further purification unless otherwise described. The antimetabolic peptide with an extra linkage containing glycine and cysteine residues (AP-SH) was synthesized by the GenScript (Nanjing) Co., Ltd. Tubulin was purchased from Cytoskeleton Inc. (tubulin protein (>99% purity), source: porcine brain, Cat. # T240, white solid) and was stored at 4 °C before reconstitution. Subsequently, the reconstitution was carried out with general tubulin buffer (80 mM piperazine-*N,N'*-bis(2-ethanesulfonic acid) (PIPES), 2 mM MgCl<sub>2</sub>, 0.5 mM ethylene glycol-bis( $\beta$ -aminoethyl ether)-*N,N,N',N'*-tetraacetic acid (EGTA), 5% glycerol, 1 mM guanosine 5'-triphosphate (GTP), pH 6.9) and the initial concentration was 10 mg/mL. The preparative solution was aliquoted and stored in liquid nitrogen and store at –70 °C. After diluting into the experiment concentration, tubulin was resuspended in the buffer solution and put under 37 °C for 15 min. Typically, the molar equivalent of tubulin is defined as the heterodimer that has a molecular weight of 110 kDa. All compounds are >95% pure by high-performance liquid chromatography (HPLC) analysis.

**Instruments.** NMR spectra were recorded on Bruker 400 MHz instrument in D<sub>2</sub>O, and all of the chemical shifts were recorded in parts per million (ppm). High-resolution mass spectra (HRMS) were performed on a Varian 7.0T FTMS with electrospray ionization (ESI) or matrix-assisted laser desorption ionization (MALDI) source. TEM images were acquired with a high-resolution transmission electron microscope (Philips Tecnai G2 20S-TWIN microscope) operating at an accelerating voltage of 200 keV. The samples were prepared by placing a drop of solution onto a carbon-coated copper grid and air-dried. The initial concentrations for the preparation of TEM samples were provided in the main text. The morphological information was directly obtained from the fresh TEM samples without staining. The spectrum of the UV–vis titration and fluorescence titrations were recorded on a Shimadzu UV-3600 spectrophotometer and Varian Cary Eclipse spectrophotometer at 37 °C. The transmission spectra were recorded on a Shimadzu UV-3600 spectrophotometer in a quartz cell (light path 10 mm) at 37 °C with a PTC-348WI temperature controller. Dynamic light scattering (DLS) was recorded

on BI-200SM (Brookhaven Company) at 37 °C. Fluorescence imaging experiments were carried out by a home-built objective-type total internal reflection fluorescence microscopy (TIRFM) imaging system. Specifically, a Ti-U inverted epifluorescence microscope (Nikon, Tokyo, Japan) was equipped with a 100× total internal reflection fluorescence (TIRF) objective (numerical aperture (NA) = 1.49) and a single-mode fiber-coupled semiconductor laser. The fluorescence signals were collected with an electron-multiplying charge-coupled device (EMCCD) (Andor iXon Ultra 897) and the exposure time was 50 ms. The electron-multiplying (EM) gain of EMCCD was set to 4–40. *In vivo* imaging observation of mice was performed using a small animal 3D optical *in vivo* imager (IVIS Lumina II). The tissues of tumors and organs were stained with H&E and observed with a fluorescence microscope (DP26, OLYMPUS, Japan). The light-emitting diodes (LEDs) mainly emit at 650 nm but cover the range from 640 to 660 nm.

**Synthesis of SMCC- $\beta$ CD.** Mono-6-NH<sub>2</sub>-PMe- $\beta$ CD (71.0 mg, 0.05 mmol), SMCC (20 mg, 0.06 mmol), and *N,N*-diisopropylethylamine (DIPEA) (22  $\mu$ L, 0.125 mmol) were added to a solution of anhydrous CH<sub>2</sub>Cl<sub>2</sub> (12 mL) under nitrogen. The obtained solution was stirred at room temperature for 18 h to give the crude product, which was purified by column chromatography using CHCl<sub>3</sub>/CH<sub>3</sub>OH = 10:1. <sup>1</sup>H NMR (400 MHz, CD<sub>3</sub>Cl)  $\delta$  = 6.68 (d, *J* = 4.6, 2H), 5.14–5.07 (m, 7H), 3.86–3.77 (m, 14H), 3.70–3.52 (m, 35H), 3.51–3.43 (m, 25H), 3.42–3.25 (m, 21H), 3.20–3.09 (m, 7H), 2.80 (s, 2H), 2.14 (m, 1H), 2.00 (s, 1H), 1.86 (m, 2H), 1.74–1.70 (s, 2H), 1.28–1.23 (m, 2H), 1.02–0.96 (m, 2H), <sup>13</sup>C NMR (100 MHz, CD<sub>3</sub>Cl)  $\delta$  = 174.7, 170.0, 133.0, 98.0, 98.0, 97.9, 97.8, 97.6, 97.6, 81.1, 81.0, 81.0, 80.8, 80.8, 80.7, 80.6, 80.4, 79.5, 79.3, 79.0, 78.9, 78.8, 70.6, 70.5, 70.4, 70.2, 70.1, 70.0, 70.0, 69.9, 69.9, 68.8, 60.6, 60.5, 60.4, 60.4, 60.3, 60.3, 60.2, 58.4, 58.1, 58.0, 58.0, 57.7, 57.6, 57.5, 57.5, 57.4, 57.3, 44.2, 42.6, 38.6, 35.4, 28.9, 28.3, 28.0, 27.9, 27.0, 24.6. HRMS (MALDI) *m/z* for C<sub>74</sub>H<sub>124</sub>N<sub>2</sub>O<sub>37</sub> calcd [M + Na]<sup>+</sup>: 1655.7728, found: 1655.7778. HPLC purity: 95.2%.

**Synthesis of AP-CD.** SMCC- $\beta$ CD (16.0 mg, 9.6  $\mu$ mol) and AP-SH (10.0 mg, 8  $\mu$ mol) were dissolved in PBS (0.1 M, pH = 7.2, 5.0 mL). The mixture was stirred at 25 °C for 6 h. The structural characterization of AP-CD was performed by HPLC (Thermo Scientific UltiMate 3000, using water and acetonitrile containing 0.03% of trifluoroacetic acid (TFA) as eluents) and MALDI-TOF (Varian 7.0T FTMS) spectroscopy, *m/z* for C<sub>131</sub>H<sub>208</sub>N<sub>18</sub>O<sub>51</sub>S calcd [M + Na]<sup>+</sup>: 2904.3849, found: 2904.1794. HPLC purity: 98.6%.

**Fluorescence Imaging and Colocalization Experiments.** The slides and coverslips used in the experiments were soaked in piranha solution at 80 °C for 90 min, rinsed with plenty of deionized (DI) water, and dried for use in the experiments.

For fluorescence imaging experiments, tubulin solution (1 mg/mL) was diluted 50-fold with deionized (DI) water, and then it was mixed with an equal volume of ThT solution (20 nM). After 2 min, the mixture was pipetted for imaging. The fluorescence from ThT was excited using a 450 nm laser (SFOLT Co., Ltd., China) in conjunction with a 505 nm dichroic mirror and a 515–555 nm band-pass filter (Semrock). Similarly, other solutions including tubulin/TCPP, AP-CD@tubulin, and (TCPPCAP-CD)@tubulin were diluted to the same tubulin concentration with deionized (DI) water and imaged.

For the colocalization experiment, tubulin solution (1 mg/mL) was diluted 50-fold with deionized (DI) water, and then it was mixed with an equal volume of ThT solution (20 nM). After 2 min, the mixture was pipetted for imaging. After we observed the microtubule under a microscope, it was mixed with an equal volume of AP-CD (50  $\mu$ M) for 30 min, followed by an equal volume of TCPP (25  $\mu$ M), and after 2 min, the mixture was pipetted for imaging. The fluorescence from TCPP was excited using a 532 nm laser (Changchun New Industries Optoelectronics Technology Co., Ltd., Changchun, China) in conjunction with a 565 nm dichroic mirror and a 605–660 nm band-pass filter (Semrock).

**Cell-Staining Experiments.** To observe the intracellular distribution of the tubulin cytoskeleton, A549 cells were treated with AP-CD (20  $\mu$ M), R8-TPP (10  $\mu$ M), or AP-CD (20  $\mu$ M) plus

R8-TPP (10  $\mu$ M) for 24 h. The cells were then incubated with 1 mL of the final staining solution (0.5  $\mu$ L of Pluronic F-127 (20% solution in dimethyl sulfoxide (DMSO)) to 0.5  $\mu$ L of Tubulin Tracker Green stock solution in 1 mL of live cell compatible buffer plus DAPI) for 60 min at 37 °C and 5% CO<sub>2</sub>. Then, the cells were rinsed three times in a wash buffer such as live-cell imaging solution at 37 °C (1 $\times$  probenecid was added to the wash buffer to minimize the efflux of the probe during the rinsing and imaging steps). The stained cells were then observed with a confocal microscope (FV1000, Olympus, Japan).

**Cell Viability Assay.** To investigate the toxicities of AP-CD, R8-TPP, and their complexes to the A549 cells, the cells were cultured in 96-well plates in F12 medium containing 10% FBS for 24 h in the dark or light, and then the corresponding samples were added to the wells. Cell growth was examined using a cell counting kit-8 (CCK-8) assay kit (Dojindo, Japan). The half-maximal inhibitory concentration (IC<sub>50</sub>) of complex R8-TPP/AP-CD was calculated by SPSS software. In the dark, the IC<sub>50</sub> is 29.3  $\mu$ M. Otherwise, when in light, the IC<sub>50</sub> is 16.5  $\mu$ M.

**Inhibition Experiments of Tumor Growth.** Four-week-old Balb/c nude mice ( $n = 24$ , Beijing Vital River Laboratory Animal Technology Co., Ltd., China) received 10<sup>7</sup>/mL A549 cells in PBS (100  $\mu$ L) into the right armpit by subcutaneous injection. After 15 days after tumor implantation, the mice were randomly divided into six groups (four mice per group). The groups were treated with 100  $\mu$ L PBS, AP-CD, R8-TPP, R8-TPP, R8-TPP/AP-CD, and R8-TPP/AP-CD ([AP-CD] = 2[R8-TPP] = 2 mM). All solutions were prepared in ultrapure water, which was sonicated for 30 min to uniformly disperse and dissolve. Then, they were stored in a 4 °C refrigerator and protected from light for further use.

On the second day after the drug was injected, two groups of mice were irradiated with a 660 nm laser for 3 min at the tumor site. After 9 days of treatment, the body weight and tumor changes of the mice were continued to be observed. The tumor volumes ( $V$ ) were measured using a Vernier caliper every 2 days and calculated using the following equation:  $V = 0.5 \times (\text{tumor length}) \times (\text{tumor width})^2$ . The relative tumor volumes were calculated as  $V/V_0$  ( $V_0$  is the tumor volume when the drug injection begins). The tissues of tumors and organs were stained with H&E and observed. All experimental procedures were approved and in accordance with China's National Code of Animal Care for Scientific Experimentation. The experiments were also assessed by the Animal Experimentation Ethics Committee of Nankai University, and the assigned approval number is 2021-SYDELL-000448.

## ■ ASSOCIATED CONTENT

### Supporting Information

The Supporting Information is available free of charge at <https://pubs.acs.org/doi/10.1021/acs.jmedchem.2c01398>.

Compound characterization, rotating frame nuclear Overhauser effect spectroscopy (ROESY) spectra; photoluminescence spectrum; optical transmittance; diameter distributions; UV–vis spectra; and confocal fluorescence images (PDF)

Molecular formula string (CSV)

## ■ AUTHOR INFORMATION

### Corresponding Authors

**Ying-Ming Zhang** – College of Chemistry, State Key Laboratory of Elemento-Organic Chemistry, Nankai University, Tianjin 300071, P. R. China; Email: [ymzhang@nankai.edu.cn](mailto:ymzhang@nankai.edu.cn)

**Lehui Xiao** – State Key Laboratory of Medicinal Chemical Biology, Tianjin Key Laboratory of Biosensing and Molecular Recognition, College of Chemistry, Nankai University, Tianjin 300071, P. R. China; Email: [lehuixiao@nankai.edu.cn](mailto:lehuixiao@nankai.edu.cn)

**Yu Liu** – College of Chemistry, State Key Laboratory of Elemento-Organic Chemistry, Nankai University, Tianjin 300071, P. R. China; Haihe Laboratory of Sustainable Chemical Transformations, Tianjin 300192, P. R. China; [orcid.org/0000-0001-8723-1896](https://orcid.org/0000-0001-8723-1896); Email: [yuliu@nankai.edu.cn](mailto:yuliu@nankai.edu.cn)

## Authors

**Mian Tang** – College of Chemistry, State Key Laboratory of Elemento-Organic Chemistry, Nankai University, Tianjin 300071, P. R. China

**Yao-Hua Liu** – College of Chemistry, State Key Laboratory of Elemento-Organic Chemistry, Nankai University, Tianjin 300071, P. R. China

**Hua Liu** – State Key Laboratory of Medicinal Chemical Biology, Tianjin Key Laboratory of Biosensing and Molecular Recognition, College of Chemistry, Nankai University, Tianjin 300071, P. R. China

**Qiyue Mao** – Department of Molecular Chemistry and Biochemistry, Doshisha University, Kyoto 610-0321, Japan

**Qilin Yu** – Key Laboratory of Molecular Microbiology and Technology, College of Life Sciences, Nankai University, Tianjin 300071, P. R. China

**Hiroaki Kitagishi** – Department of Molecular Chemistry and Biochemistry, Doshisha University, Kyoto 610-0321, Japan; [orcid.org/0000-0003-4682-7217](https://orcid.org/0000-0003-4682-7217)

Complete contact information is available at:

<https://pubs.acs.org/10.1021/acs.jmedchem.2c01398>

## Author Contributions

<sup>#</sup>M.T. and Y.-H.L. contributed equally to this work.

## Notes

The authors declare no competing financial interest.

## ■ ACKNOWLEDGMENTS

This work was financially supported by the National Natural Science Foundation of China (grants 21871154, 22171148, 22131008, 22174079, and 21974073), the Natural Science Foundation of Tianjin (21JCZDJC00310), the Fundamental Research Funds for the Central Universities (Nankai University), and the Haihe Laboratory of Sustainable Chemical Transformation.

## ■ ABBREVIATIONS USED

AP-CD, antimetastatic polypeptide-modified permethyl  $\beta$ -cyclodextrin; R8-TPP, octaarginine-conjugated tetraphenylporphyrin; SMCC- $\beta$ CD, SMCC-modified permethyl  $\beta$ -cyclodextrin; AP-SH, thiol-modified antimetastatic polypeptide

## ■ REFERENCES

- (1) Zhang, Y.-M.; Liu, Y.-H.; Liu, Y. Supramolecular Nanoassemblies Based on Proteins and Cyclodextrin Derivatives. In *Supramolecular Protein Chemistry: Assembly, Architecture and Application*; Crowley, P. B., Ed.; Royal Society of Chemistry: Cambridge, 2020; pp 124–160.
- (2) Sun, C.; Wang, Z.; Yue, L.; Huang, Q.; Cheng, Q.; Wang, R. Supramolecular Induction of Mitochondrial Aggregation and Fusion. *J. Am. Chem. Soc.* **2020**, *142*, 16523–16527.
- (3) Yang, K.; Qi, S.; Yu, X.; Bai, B.; Zhang, X.; Mao, Z.; Huang, F.; Yu, G. A Hybrid Supramolecular Polymeric Nanomedicine for Cascade-Amplified Synergetic Cancer Therapy. *Angew. Chem., Int. Ed.* **2022**, No. e202203786.

- (4) Sun, C.; Wang, Z.; Yang, K.; Yue, L.; Cheng, Q.; Ma, Y.-l.; Lu, S.; Chen, G.; Wang, R. Polyamine-responsive Morphological Transformation of a Supramolecular Peptide for Specific Drug Accumulation and Retention in Cancer Cells. *Small* **2021**, *17*, No. 2101139.
- (5) Yang, X.; Wang, R.; Kermagoret, A.; Bardelan, D. Oligomeric Cucurbituril Complexes: from Peculiar Assemblies to Emerging Applications. *Angew. Chem., Int. Ed.* **2020**, *59*, 21280–21292.
- (6) Majumdar, S.; Wang, X.; Sommerfeld, S. D.; Chae, J. J.; Athanopoulou, E.-N.; Shores, L. S.; Duan, X.; Amzel, L. M.; Stellacci, F.; Schein, O.; Guo, Q.; Singh, A.; Elisseff, J. H. Cyclodextrin Modulated Type I Collagen Self-Assembly to Engineer Biomimetic Cornea Implants. *Adv. Funct. Mater.* **2018**, *28*, No. 1804076.
- (7) Sun, Y.; Ma, J.; Zhang, F.; Zhu, F.; Mei, Y.; Liu, L.; Tian, D.; Li, H. A Light-regulated Host-guest-based Nanochannel System Inspired by Channelrhodopsins Protein. *Nat. Commun.* **2017**, *8*, No. 260.
- (8) Liu, Y.-H.; Liu, Y. Highly Effective Gene Delivery Based on Cyclodextrin Multivalent Assembly in Target Cancer Cells. *J. Mater. Chem. B* **2022**, *10*, 958–965.
- (9) Zhang, Y.-M.; Zhang, N.-Y.; Xiao, K.; Yu, Q.; Liu, Y. Photo-Controlled Reversible Microtubule Assembly Mediated by Paclitaxel-Modified Cyclodextrin. *Angew. Chem., Int. Ed.* **2018**, *57*, 8649–8653.
- (10) Zhang, Y.-M.; Liu, J.-H.; Yu, Q.; Wen, X.; Liu, Y. Targeted Polypeptide–Microtubule Aggregation with Cucurbit[8]uril for Enhanced Cell Apoptosis. *Angew. Chem., Int. Ed.* **2019**, *58*, 10553–10557.
- (11) Liu, Y.-H.; Zhang, Y.-M.; Yu, H.-J.; Liu, Y. Cucurbituril-Based Biomacromolecular Assemblies. *Angew. Chem., Int. Ed.* **2021**, *60*, 3870–3880.
- (12) Zhang, Q.; Zhang, J.; Song, J.; Liu, Y.; Ren, X.; Zhao, Y. Protein-Based Nanomedicine for Therapeutic Benefits of Cancer. *ACS Nano* **2021**, *15*, 8001–8038.
- (13) Zhang, N.; Mei, K.; Guan, P.; Hu, X.; Zhao, Y. Protein-Based Artificial Nanosystems in Cancer Therapy. *Small* **2020**, *16*, No. 1907256.
- (14) Tang, M.; Liu, Y.-H.; Xu, X.-M.; Zhang, Y.-M.; Liu, Y. Dual-Responsive Drug Release and Fluorescence Imaging Based on Disulfide-Pillar[4]arene Aggregate in Cancer Cells. *Bioorg. Med. Chem.* **2022**, *57*, No. 116649.
- (15) Shi, B.; Jie, K.; Zhou, Y.; Zhou, J.; Xia, D.; Huang, F. Nanoparticles with Near-Infrared Emission Enhanced by Pillararene-Based Molecular Recognition in Water. *J. Am. Chem. Soc.* **2016**, *138*, 80–83.
- (16) Zhang, Q.; Liu, F.; Nguyen, K. T.; Ma, X.; Wang, X.; Xing, B.; Zhao, Y. Multifunctional Mesoporous Silica Nanoparticles for Cancer-Targeted and Controlled Drug Delivery. *Adv. Funct. Mater.* **2012**, *22*, 5144–5156.
- (17) Kitagishi, H.; Jiomaru, M.; Hasegawa, N. Intracellular Delivery of Adamantane-Tagged Small Molecule, Proteins, and Liposomes Using an Octaarginine-Conjugated  $\beta$ -Cyclodextrin. *ACS Appl. Bio Mater.* **2020**, *3*, 4902–4911.
- (18) Tang, M.; Song, Y.; Lu, Y.-L.; Zhang, Y.-M.; Yu, Z.; Xu, X.; Liu, Y. Cyclodextrin-Activated Porphyrin Photosensitization for Boosting Self-Cleavable Drug Release. *J. Med. Chem.* **2022**, *65*, 6764–6774.
- (19) Chen, H.; Zeng, X.; Tham, H. P.; Phua, S. Z. F.; Cheng, W.; Zeng, W.; Shi, H.; Mei, L.; Zhao, Y. NIR-Light-Activated Combination Therapy with a Precise Ratio of Photosensitizer and Prodrug Using a Host–Guest Strategy. *Angew. Chem., Int. Ed.* **2019**, *58*, 7641–7646.
- (20) Tian, J.; Xia, L.; Wu, J.; Huang, B.; Cao, H.; Zhang, W. Linear Alternating Supramolecular Photosensitizer for Enhanced Photodynamic Therapy. *ACS Appl. Mater. Interfaces* **2020**, *12*, 32352–32359.
- (21) Chen, H.; Yang, J.; Sun, L.; Zhang, H.; Guo, Y.; Qu, J.; Jiang, W.; Chen, W.; Ji, J.; Yang, Y.-W.; Wang, B. Synergistic Chemotherapy and Photodynamic Therapy of Endophthalmitis Mediated by Zeolitic Imidazolate Framework-Based Drug Delivery Systems. *Small* **2019**, *15*, No. 1903880.
- (22) Nguyen, L.; Li, M.; Woo, S.; You, Y. Development of Prodrugs for PDT-Based Combination Therapy Using a Singlet-Oxygen-Sensitive Linker and Quantitative Systems Pharmacology. *J. Clin. Med.* **2019**, *8*, No. 2198.
- (23) Jo, S.-M.; Kim, H. S.; Won, M.; Champanhac, C.; Kim, J. S.; Wurm, F. R.; Landfester, K. Dual-Targeted Nanoreactors and Prodrugs: Hydrogen Peroxide Triggers Oxidative Damage and Prodrug Activation for Synergistic Elimination of Cancer Cells. *Adv. Funct. Mater.* **2022**, *32*, No. 2200791.
- (24) Pieraccini, S.; Saladino, G.; Cappelletti, G.; Cartelli, D.; Francescato, P.; Speranza, G.; Manitto, P.; Sironi, M. In Silico Design of Tubulin-targeted Antimitotic Peptides. *Nat. Chem.* **2009**, *1*, 642–648.
- (25) Sun, M.; Wang, C.; Lv, M.; Fan, Z.; Du, J. Intracellular Self-Assembly of Peptides to Induce Apoptosis against Drug-Resistant Melanoma. *J. Am. Chem. Soc.* **2022**, *144*, 7337–7345.
- (26) Kitagishi, H.; Hatada, S.; Itakura, T.; Maki, Y.; Maeda, Y.; Kano, K. Cellular Uptake of Octaarginine-conjugated Tetraarylporphyrin Included by Per-O-methylated  $\beta$ -Cyclodextrin. *Org. Biomol. Chem.* **2013**, *11*, 3203–3211.
- (27) Kitagishi, H.; Saito, M.; Mao, Q.; Kiriya, A.; Negi, S.; Kano, K. Supramolecular Complexation in Biological Media: NMR Study on Inclusion of an Anionic Tetraarylporphyrin into a Per-O-Methylated  $\beta$ -Cyclodextrin Cavity in Serum, Blood, and Urine. *Chem.—Asian J.* **2019**, *14*, 3320–3328.
- (28) Ye, Z.; Geng, X.; Wei, L.; Li, Z.; Lin, S.; Xiao, L. Length-Dependent Distinct Cytotoxic Effect of Amyloid Fibrils beyond Optical Diffraction Limit Revealed by Nanoscopic Imaging. *ACS Nano* **2021**, *15*, 934–943.
- (29) Yu, L.; Zhang, W.; Luo, W.; Dupont, R. L.; Xu, Y.; Wang, Y.; Tu, B.; Xu, H.; Wang, X.; Fang, Q.; Yang, Y.; Wang, C. Molecular Recognition of Human Islet Amyloid Polypeptide Assembly by Selective Oligomerization of Thioflavin T. *Sci. Adv.* **2020**, *6*, No. eabc1449.

## Recommended by ACS

### Microtubule-Targeted Self-Assembly Triggers Prometaphase–Metaphase Oscillations Suppressing Tumor Growth

Guanying Li, Ye Zhang, *et al.*

MARCH 23, 2021  
NANO LETTERS

[READ !\[\]\(fc3a57079704ef1b99671c8cafae23be\_img.jpg\)](#)

### Triglyceride-Mimetic Structure-Gated Prodrug Nanoparticles for Smart Cancer Therapy

Chutong Tian, Jin Sun, *et al.*

NOVEMBER 01, 2021  
JOURNAL OF MEDICINAL CHEMISTRY

[READ !\[\]\(d5831b2ac75eb48b4c49d27e61d24c03\_img.jpg\)](#)

### Glutathione and Reactive Oxygen Species Dual-Responsive Block Copolymer Prodrugs for Boosting Tumor Site-Specific Drug Release and Enhanced Antitumor Efficacy

Wei Yin, Zhishen Ge, *et al.*

JANUARY 21, 2020  
BIOMACROMOLECULES

[READ !\[\]\(e97636a3328cdaccd5ffd8fe3bc69ce6\_img.jpg\)](#)

### PDTAC: Targeted Photodegradation of GPX4 Triggers Ferroptosis and Potent Antitumor Immunity

Sijin Liu, Guoquan Liu, *et al.*

SEPTEMBER 06, 2022  
JOURNAL OF MEDICINAL CHEMISTRY

[READ !\[\]\(64aa49a093b417cefcbea2338d3c32ec\_img.jpg\)](#)

[Get More Suggestions >](#)